Graphenated tantalum(IV) oxide and poly(4-styrene sulphonic acid)-doped polyaniline nanocomposite as cathode material in an electrochemical capacitor

Article *in* Portugaliae Electrochimica Acta · January 2014

DOI: 10.1016/j.electacta.2013.12.15

CITATIONS
7

READS
46

14 authors, including:

Christopher Edozie Sunday
University of the Western Cape
22 PUBLICATIONS **110** CITATIONS
SEE PROFILE

Tesfaye T. Waryo
University of the Western Cape
53 PUBLICATIONS **460** CITATIONS
SEE PROFILE

Milua Masikini
University of the Western Cape
21 PUBLICATIONS **168** CITATIONS
SEE PROFILE

Nolubabalo Matinise
University of the Western Cape
20 PUBLICATIONS **180** CITATIONS
SEE PROFILE

Electrochimica Acta 128 (2014) 226–237

Contents lists available at ScienceDirect

Electrochimica Acta

journal homepage: www.elsevier.com/locate/electacta

Graphenated tantalum(IV) oxide and poly(4-styrene sulphonic acid)-doped polyaniline nanocomposite as cathode material in an electrochemical capacitor

Njagi Njomo[a], Tesfaye Waryo[a], Milua Masikini[a], Chinwe O. Ikpo[a], Stephen Mailu[a], Oluwakemi Tovide[a,b], Natasha Ross[a], Avril Williams[b], Nolubabalo Matinise[a], Christopher E. Sunday[a], Noluthando Mayedwa[a], Priscilla G.L. Baker[a], Kenneth I. Ozoemena[c], Emmanuel I. Iwuoha[a,*]

[a] SensorLab, Department of Chemistry, University of the Western Cape, Robert Sobukwe Road, Bellville, South Africa
[b] Department of Biological and Chemical Sciences, University of the West Indies, Cave Hill, Barbados
[c] Council for Scientific and Industrial Research (CSIR), Pretoria, South Africa

ARTICLE INFO

Article history:
Received 24 July 2013
Received in revised form
17 December 2013
Accepted 19 December 2013
Available online 7 January 2014

Keywords:
Tantalum(IV) oxide
Polyaniline
Poly(4-styrene sulphonic) acid
Nanocomposite

ABSTRACT

Nanostructured poly(4-styrene sulphonic acid) and tantalum (IV) oxide-doped polyaniline nanocomposite were synthesised and their electro-conductive properties were determined. The oxide was synthesized using a modified sol-gel method and then dispersed in acidic media through sonication and entrapped *in-situ* into the polymeric matrix during the oxidative chemical polymerization of aniline doped with poly(4-styrene sulphonic acid). The oxides and novel polymeric nanocomposite were characterised with TEM, SEM, EDX, XRD, FTIR, UV-visible to ascertain elemental and phase composition, successful polymerization, doping, morphology and entrapment of the metal oxide nanoparticles. The electro-conductivity of the nanomaterial was interrogated using scanning electrochemical microscopy (SECM) and cyclic voltammetry (CV). The material was then anchored on activated graphitic carbon and used in the design of an asymmetric supercapacitor cell using 6 M KOH aqueous electrolyte. Characteristically high specific capacitance values of 318.4 F/g with a corresponding energy and power densities of 1.57 kWh/kg and 0.435 kW/kg, respectively, were demonstrated. The cell also showed high coulombic efficiency of 94.9% with a long cycle life and good cycle stability making the nanomaterial suitable for constructing supercapacitor cell electrodes.

1. Introduction

In storing and sustaining renewable energy, current research and development efforts on electrochemical energy devices are focused mainly on fuel cells, batteries and supercapacitors. These efforts are geared towards achieving high specific energy, high specific power, long cycle life, small size, light weight and relatively low cost [1,2]. Due to their unique characteristics of high specific capacitance, high power density, low self-discharge, safe operation, high cycling stability and fast charge/discharge capability, supercapacitors have attracted enormous interests and are considered to be among the most promising energy conversion and energy storage devices to fulfil future energy demands [3–5]. Their characteristics are being exploited in applications ranging from power electronics, large scale transport systems comprising subway trains, aeroplanes and buses to energy storage at intermittent generators including windmills, solar and smart grid applications. Depending on the energy storage mechanism, supercapacitors have been categorized into two types: electrochemical double layer capacitors (EDLCs) and pseudocapacitors. In EDLCs, energy is stored electrostatically as negative and positive electric charges in an electrochemical double layer electrode-electrolyte interface through a non-faradaic process, prompting a rapid response and reversibility of the interface to changes in electrode potentials. Pseudocapacitors on the other hand are based on electrode charge storage mechanism requiring highly reversible surface faradaic redox processes across an electrode-electrolyte interface involving electroactive electrode materials [3,6–8]. The two mechanisms can function simultaneously depending on the nature of the electrode materials [5]. EDLCs use carbon-based active materials and represent attractive high power and durable energy storage devices because of their often-cited desirable physical and chemical properties which include low cost, ease of processability, high conductivity, accessibility, controllable porosity with various

* Corresponding author.
E-mail address: eiwuoha@uwc.ac.za (E.I. Iwuoha).

0013-4686/$ – see front matter © 2014 Elsevier Ltd. All rights reserved.
http://dx.doi.org/10.1016/j.electacta.2013.12.150

surface functionalities, variety of forms attainable (fibers, powders, sheets, aerogels, composites, monoliths, tubes, foams, fibres, onions, nanohorns, etc), relatively inert electrochemistry and electroactive sites for a variety of redox reactions [5,6,9,10]. A proper control over the specific surface area and the pore size adaptable to an appropriate type of electrolyte solution are crucial to ensuring good performance of EDLCs in terms of both power delivery rate and energy storage capacity because high ability charge accumulation at the interface depends upon the availability and wettability of pores with dimensions adaptable to the size of solvated anions and cations which have to be transported from the bulk of the electrolyte [5,11]. In addition to high-surface-area carbon materials, higher capacitances can be achieved by using redox-active transition metal oxides and conducting polymers. Due to existence of variable oxidation-state structures over potential ranges, pseudocapacitive transition-metal oxides electrode materials have been found to exhibit high energy density and large charge transfer-reaction pseudocapacitance based on fast and reversible redox reactions at the electrode surface [12]. Electronically conducting polymers (ECPs) characterized by their low cost, high specific capacitances, generally fast charge–discharge processes and high conductivities in their charged states, are promising materials for the realization of high specific energy/power performance pseudocapacitors. An advantageous characteristic of ECPs over carbon based electrodes is that charging takes place not only at the interface as is the case with carbon materials but through the whole mass of the active electrode film during doping-dedoping processes resulting in huge specific capacitance [13–15]. Ideal double layer capacitance behaviour of an electrode material expresses itself in form of a rectangular shape in a cyclic voltammetric curve. The sign of current is instantaneously reversed upon reversal of the potential sweep. Electrode materials with pseudocapacitance properties point out a deviation from such a rectangular shape and reversible redox peaks connected with pseudofaradaic reactions are remarkable. In this case the charge accumulated in the capacitor is strongly dependent on the electrode potential. The observed delay of potential during reversing the potential sweep is connected with a kinetically slow electron transfer process involved during charging the pseudocapacitance [3]. This makes double layer capacitance more efficient than pseudofaradaic capacitance, efficiency being dependant upon electron transfer process. In this work, an asymmetric supercapacitor made up of doped polyaniline dispersed activated graphite and Tantalum(IV)oxide composite was developed. The pseudocapacitance from the polymer and the metal oxide would synergise the double layer capacitance derived from activated graphite and hence produce a composite of great charge storage.

2. Experimental

2.1. Apparatus and reagents

Analytical grades tantalum ethoxide, glacial acetic acid, aniline, poly(4-styrene sulphonic acid), ammonium persulphate, absolute ethanol, sulphuric acid and polytetrafluoroethylene (PTFE) binder solution (supplied as 60% PTFE in H_2O) were all purchased from Sigma-Aldrich. Cyclic voltammetric experiments were carried using a BAS 100 W integrated and automated electrochemical workstation from BioAnalytical Systems, Lafayette, USA. The voltammograms were recorded with a computer interfaced to the BAS 100 W electrochemical workstation. A 10 mL electrochemical cell with a conventional three electrode setup was used. The electrodes were: (1) glassy carbon working electrode from Bio Analytical Systems, either bare or modified with study material; (2) platinum wire, from Sigma Aldrich, used as a counter electrode; and (3) Ag/AgCl (3 M KCl type) from BAS was the reference electrode. Transmission electron microscopy (TEM) and Energy Dispersive X-ray (EDX) spectroscopic analysis of nanomaterial mounted on a copper coated or carbon membrane grid were performed with a Tecnai G2 F20X-Twin MAT 200 kV Field Emission Transmission Electron Microscope from FEI (Eindhoven, Netherlands). The TEM and EDX specimens were prepared by dispersing an arbitrary amount of solid in ethanol by ultrasonic treatment. A few drops were poured onto a porous carbon membrane or on a copper grid, and then dried in ambient temperatures. SEM image was obtained using a low resolution HITACHI X-650 Scanning Electron Microscopy with an electron accelerating voltage of 25 KV.

2.2. Synthesis of tantalum (IV) oxide nanoparticles

508 μL of tantalum ethoxide was mixed with 2.532 mL of absolute ethanol in a 50 mL bottle and stirred for 30 min. 191 μL of glacial acetic acid was slowly added with slow stirring. The content was stirred for 2 h to form a white gel. The gel was transferred to 50 mL falcon tubes and centrifuged for 15 min at 6000 rpm. It was washed with absolute ethanol by adding the ethanol to the residual, mechanically shaking and centrifuging again and discarding the supernatant. The residual is dried in vacuum furnace at 45 °C for 12 h then 120 °C for 4 h. It is then annealed at 350 °C in a box furnace for 3 h. The calcinations product was characterised with TEM, EDX and XRD for morphological and elemental constituents. The product was then used in the *in-situ* synthesis of the polymeric nanocomposite with polyaniline.

2.3. Synthesis of poly(4-styrene sulphonic) acid and tantalum (IV) oxide doped polyaniline nanocomposite

The synthesis of the polymeric nanocomposites was done by ultrasonic dispersion and polymerization of aniline. 0.225 g of tantalum (IV) oxide nanoparticles was weighed and added to 100 mL of 2 M HCl in a 200 mL bottle to which 4.5 mL of poly-(4-styrene sulphonic acid) was added. The mixture was sonicated for 30 min and then transferred to an ice-bath maintained at between 0-5 °C. 2 mL of aniline and 1.165 g of ammonium persulphate were added to the mixture and stirred for 1 h using a magnetic stirrer. The mixture was left standing for 4 h in ice-bath and then out of the bath for 48 h. Two distinct layers of a solid that settled at the bottom and a supernatant liquid formed. The upper liquid layer was slowly decanted and discarded. The residual was washed thoroughly by adding a large amount of ultra-pure distilled de-ionized water, mechanically shaking, centrifuging the mixture for 15 min at 6000 rpm and discarding the upper solution layer. The washing was done three times and lastly repeated with ethanol. The product was dried at 45 °C for 4 h under vacuum then at 78 °C for 12 h. The solid product was characterised using TEM, SEM, EDX, XRD, CV, FTIR and UV-Visible. It was then used to fabricate a supercapacitor electrode.

2.4. Oxidative pre-treatment of graphitic carbon and its integration with tantalum (IV) oxide -PANi-PSSA

Oxidative pre-treatment of graphitic carbon was undertaken to functionalise the graphite. This was done following a protocol adopted from literature [15–17] in which 5.0 g of graphitic carbon was weighed and sonicated for 7 h in a mixture of 150 mL conc. HNO_3 and 50 mL conc. H_2SO_4 (acid ratio = 3:1). The mixture was left standing overnight. Two layers were formed; a solid layer settling at the bottom and a supernatant liquid forming at the top. The supernatant liquid was decanted slowly. The oxidized graphite residual was extensively washed with de-ionised water by adding 50 mL of water in a plastic bottle, mechanically shaking the mixture and centrifuging at 6000 revolutions per minute (rpm) for 15 min

using a centrifuging machine model EBA 21 Hettich ZENTRIFUGEN. This washing was repeated until the washings ran neutral at pH 7. The sample was dried under vacuum overnight at a temperature of 55 °C prior to use. The composite, activated graphite and the surfactant hexadecylcetyltrimethylammonium bromide (CTAB) were then weighed in a mass:mass:mass ratio of 1:1:2 and added to a glass bottle. 100 mL of water was added and the bottle was closed. The content was placed in a silicone oil bath and the temperature was adjusted to 80 °C. The content was stirred for 48 h in a closed system using magnetic stirring. The mixture was filtered in vacuum and repeatedly washed with distilled de-ionised water 5 times to get rid of the surfactant. The solid was dried under vacuum overnight at 45 °C.

2.5. Fabrication of electrode

2.5.1. Preparation of electrode materials

The material used in the experiment for fabrication of the electrode consisted of 90% wt active material and 10% wt polytetrafluoroethylene (PTFE) bidder [18]. The active material consisted of chemically synthesized tantalum (IV) oxide-PANi-PSSA. 0.225 g of the nanomaterial and appropriate volume of bidder was measured and dispersed in 3 mL isopropyl alcohol in a beaker by ultrasonic shaking for 30 min to form homogeneous mixed slurry. The beaker and its content was placed on top of a hot plate at the lowest setting and constantly stirred with a cellulose rod to evaporate the solvent and further mix the components to form dough. Once the isopropyl alcohol has almost completely evaporated, the dough is transferred to a flat glass plate and using a Teflon rod, rolled into mm thin film. The prepared film was put into an oven and baked at 100 °C under vacuum for 24 h during which time the remaining isopropyl alcohol and/or moisture in the film completely evaporated. The large piece of film was cut into small wafers of about 1 cm^2 for constructing an electrode.

2.5.2. Construction of a two-electrode supercapacitor cell

A single electrode was assembled with three parts; electrode material, nickel mesh current collector and copper wire. The electrode was assembled by cutting the nickel mesh current collector into a 1 cm × 4 cm rectangular shape. The collector was then cleaned by mechanically shaking it in 1 M H_2SO_4, washing with deionised water and drying it in oven and then weighing. The approximately 1 cm^2 wafer was placed on the nickel mesh and pressed at a pressure of 20 MPa for 5 min. The electrode was then weighed and the difference in mass was used as the active mass of the electrode. The copper wire was tightly held onto the current collector using seal tape for external circuit connection. This fabrication acted as the cathode in the cell construction. The anode was made similarly save for the active material. The active material for anode electrode was activated carbon**.** The two were used to make a two-electrode asymmetric supercapacitor cell. The cell system was fabricated using 6 M KOH solution as the electrolyte and tested for the supercapacitor parameters using the BST8-3 eight-channel battery testing machine. The cell was made by holding together the two single electrodes (cathode and anode) with a porous and electronically non-conductive separator (polypropylene film) sandwiched between them to form the cell configuration.

3. 3 Results and discussion

3.1. Synthesis of tantalum (IV) oxide nanoparticles

Fig. 1 is a TEM micrograph of the calcinations product formed through the alkoxide-based sol-gel synthetic route using tantalum ethoxide as the precursor. All the organics were removed during calcination at temperatures of 350 °C.

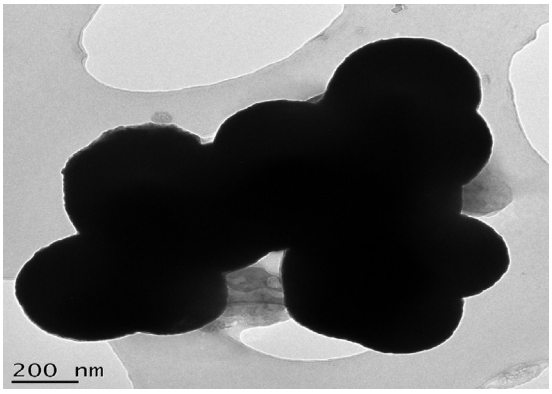

Fig. 1. TEM of tantalum (IV) oxide nanoparticles.

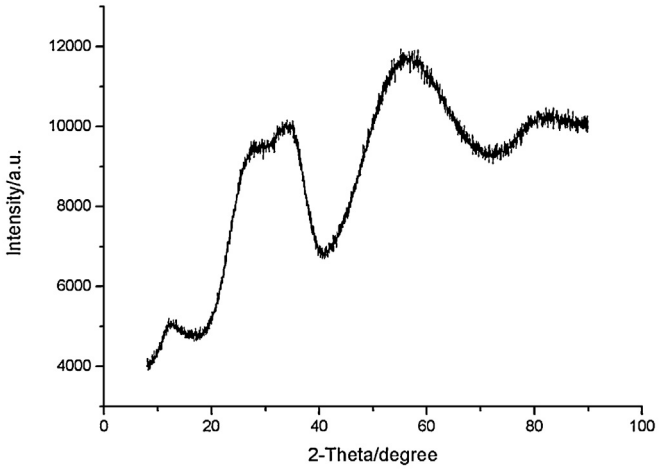

Fig. 2. XRD of tantalum (IV) oxide.

Fig. 2 is the XRD pattern of the sample showing the formation of agglomerated and amorphous tantalum (IV) oxide phase. The sol-gel chemistry in the synthesis of nanoparticles is quite complex due to the large number of reaction parameters that have to be strictly controlled such as hydrolysis and condensation, nature of the metal oxide precursors, pH, temperature, method of mixing, rate of oxidation, the nature and concentration of anions, etc, in order to provide good reproducibility of the synthesis protocol. A fundamental problem of sol-gel chemistry is that the as-synthesized precipitates are generally amorphous and the required control of their post-synthetic annealing step to induce crystallization process is a challenge that prevents any subtle control over crystal size and shape.

This constitutes a major challenge in nanoparticle synthesis and could explain the aggregation, the oversize and the amorphous nature of the tantalum (IV) oxide nanoparticles observed in this work. However, the use of non-aqueous (or non-hydrolytic) sol-gel process in an organic solvent tries to overcome some of these major limitations. They act on one hand as oxygen-supplier for the oxide formation and regulate particle size and shape as well as surface properties due to their coordination properties. In sol-gel, the as-synthesized precipitates are generally amorphous and the post-synthetic annealing step required to induce crystallization process prevents subtle control over crystal size, shape and at times the phase. As the temperature is elevated, a gel passes through various phase transitions until at some high temperature, depending on the nature of the gel, the most thermodynamically stable state is achieved [19]. Failure for this absolute control, and lack of very clear understanding of the process and very thin parameters controlling

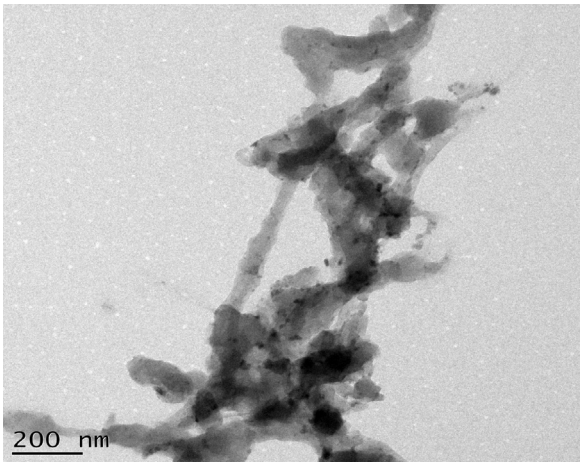

Fig. 3. TEM of tantalum (IV) oxide-PANi-PSSA.

the precipitation though helpful in improving the engineering of the growth of nanocrystals to the desired size and shape, may result in an undesirable phase formation.

3.2. Synthesis of PSSA and tantalum (IV) oxide doped polyaniline nanocomposite

Doped polyaniline (PANi) was prepared by an oxidative dispersion method. Poly(4-styrene sulphonic acid) (PSSA) was used both as a polymeric stabilizer and a dopant agent that helps in formation of colloids. When a suitable water-soluble polymer is present in the reaction mixture during the oxidation of aniline, colloidal PANi particles are obtained instead of a precipitate [20]. At the beginning of the aniline polymerization, all components of the reaction mixture, monomer (aniline), oxidant (ammonium persulfate) and steric stabilizer (PSSA) were soluble in the aqueous medium except the metal oxide suspensions. The reaction proceeds under homogeneous conditions [21]. The solution darkened gradually and acquired a blue colour over a period of about 20 min and eventually turned into dark green which is a characteristic colour of oxidized PANi. The resulting dark green dispersions were purified four times by centrifugation, filtered and washed in order to remove oligomers and excess monomers. In these approaches, the monomer is polymerized in the presence of inorganic acid particles which together with the metal oxide nanoparticles suspended act as colloidal substrate or templates for the precipitating polymer nuclei leading to the growth and formation of conducting polymer–inorganic metal oxide composite [22]. Aniline oligomers anchored at the surface stimulate and auto-accelerate the growth of PANi chains forming a film proliferating along the surface and, for steric reasons, get oriented preferentially perpendicular to the support. Practically any substrate present in the reaction mixture used for the oxidation of aniline becomes coated with a thin PANi film [20]. The successful synthesis of poly-(4-styrene-sulphonic acid) and tantalum (IV) oxide doped polyaniline nanocomposite was determined and ascertained using FTIR and TEM coupled with EDX. Fig. 3 is the TEM micrograph of tantalum (IV) oxide-PANi-PSSA showing cross-linked composite nanorods. During the 30 min sonication to disperse the composites in ethanol for TEM analysis, the oxide nanoparticles were not detached from the polymer matrix meaning that the interaction between the metal oxide nanoparticles and the polymer is strong suggesting formation of a composite. The corresponding EDX spectrum (Fig. 4) shows the elemental composition of the composite and informs of the successful synthesis of the tantalum (IV) oxide-PANi-PSSA nanocomposite. From the spectrum, all the elements in the composite were confirmed with some Cl impurities maybe from the HCl acidic media. A copper peak observed on TEM image is an impurity from the copper grid used as a support in the TEM. The presence of S, N, C and O in the EDX is a signature of successful doping of the polymer with the sulphonic acid group, $-SO_3H$. The presence of Ta and O in the EDX spectra indicates successful entrapment of the metal oxides within the polymeric network.

3.3. Scanning electron microscopy (SEM)

Fig. 5 is the SEM image of tantalum (IV) oxide-PANi-PSSA composite showing the morphological features of the nanomaterial obtained using a low resolution HITACHI X-650 Scanning Electron Microscopy with an electron accelerating voltage of 25 KV and a working distance of 15 mm. The composite display unique fibre morphology and the use of a high resolution SEM would be necessary to better interrogate and understand it. It is observed from the micrograph that the metal oxide nanoparticles are uniformly dispersed and anchored on the PANi fibre matrix.

Designing and manipulating the morphological microstructure of conducting polymer is a challenging task in materials science. It is difficult to prepare predictable polymeric nanostructures based on rational design since the morphology of a polymer is strongly affected by the nature, species, concentration of the dopant, solvent, surfactant, oxidant, and monomer, as well as the various kinds of templates and synthesis methods used. The ultimate aim in this work was to prepare tantalum (IV) oxide-PANi-PSSA nanocomposite material with high surface area morphology, a characteristic feature and requirement of electrode materials for electrochemical charge storage. The observed fibre morphology, with redox active transition metal oxide nanoparticles clearly anchored on to the redox active polymer surface, meets this criterion and can serve as good electrode materials. When integrated with activated graphitic carbon, could enhance their charge storage capacity due to an enhanced surface area and carbon functionality.

3.4. FTIR analysis of the tantalum (IV) oxide-PANi-PSSA nanocomposite

The FTIR spectrum of tantalum (IV) oxide-PANi-PSSA is shown in Fig. 6. Pure PANi is characterised by five strong bands at 1590, 1494, 1302, 1140, and 820 cm^{-1} and other weaker features or broader bands. The bands at 1590 and 1494 cm^{-1} are attributed to the C=C and C=N stretching modes of vibration for the quinoid (-N=Q=N- where Q=quinoid ring) and benzenoid units while the bands at 1302 and 1242 cm^{-1} are assigned to the C-N stretching mode of benzenoid units. The band at 1140 cm^{-1} is due to -N=Q=N- of polyaniline. The band at 820 cm^{-1} is attributed to C-C and C-H stretching for benzenoid unit of polyaniline and the one at 681.92 cm^{-1} is assigned to the out of plane C-H vibration [23]. Doping of PANi with poly(4-styrene sulphonic acid) and/or incorporation of the metal oxide nanocomposites lead to shifts in the FTIR peaks for pure PANi [24] as the results in Fig. 6 show.

Transmission maxima at 788 cm^{-1} for tantalum (IV) oxide-PANi-PSSA is consistent with the C-H out-of-plane bending motions of benzenoid rings. The 1375 cm^{-1} maxima corresponds to the C-N stretching of the secondary aromatic amine; 1217 cm^{-1} and 1326 cm^{-1} are associated with the C-H stretching vibration with aromatic conjugation; 1448 cm^{-1} is associated with C-C aromatic ring stretching vibrations of the benzenoid diamine unit; 1552 cm^{-1} arises mainly from both the stretching vibrations of N=Q=N and N-B-N rings of the quinoid (Q) and benzoid (B) units. The transmission maxima around the wave numbers 1100 cm^{-1} and 1000 cm^{-1} consistent with the presence of $-SO_3H$ group arises from asymmetric and symmetric stretching modes of S-O of the $-SO_2-O^-$ group. However, the peak around 1100 cm^{-1} in

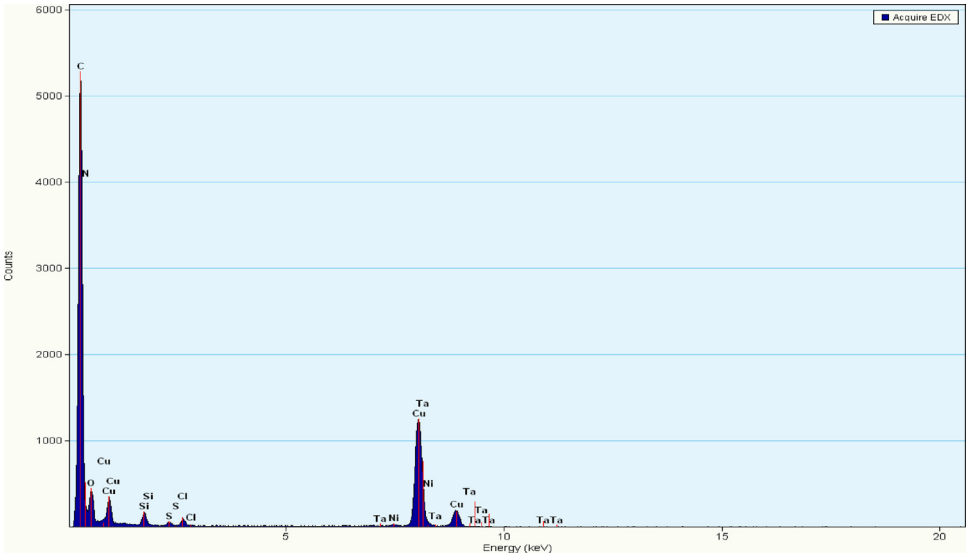

Fig. 4. EDX of tantalum (IV) oxide-PANi-PSSA.

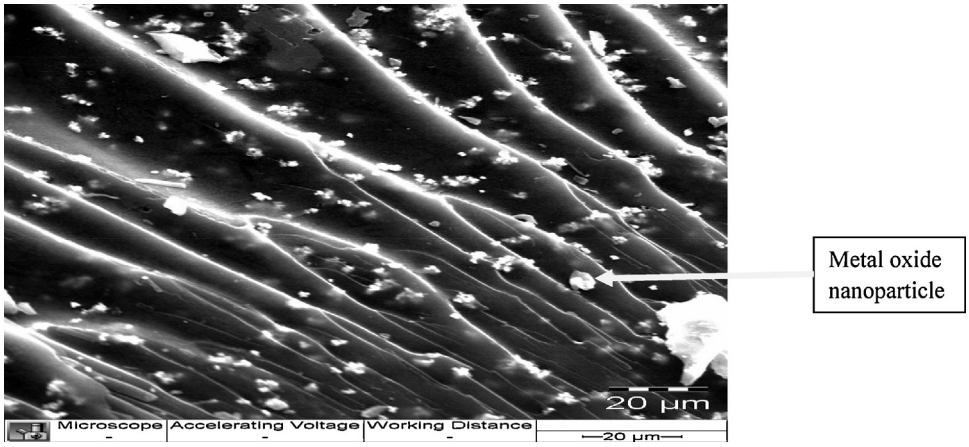

Fig. 5. SEM image of tantalum (IV) oxide-PANi-PSSA.

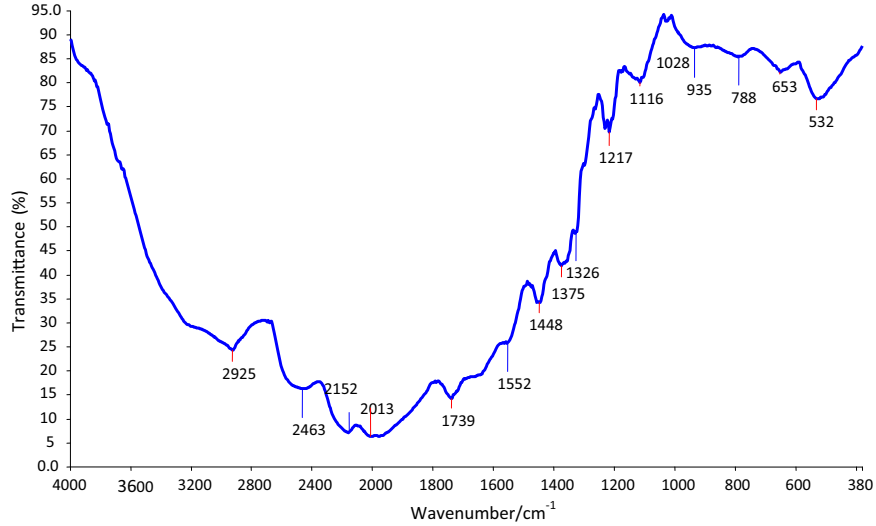

Fig. 6. FTIR of tantalum (IV) oxide-PANi-PSSA.

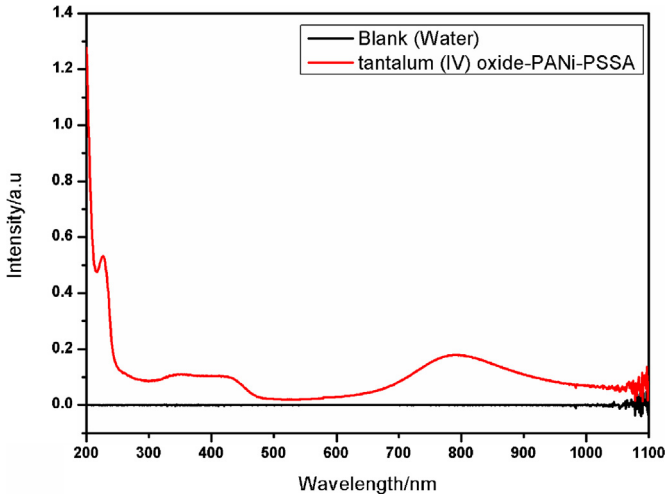

Fig. 7. UV-vis spectra of tantalum (IV) oxide-PANi-PSSA composite.

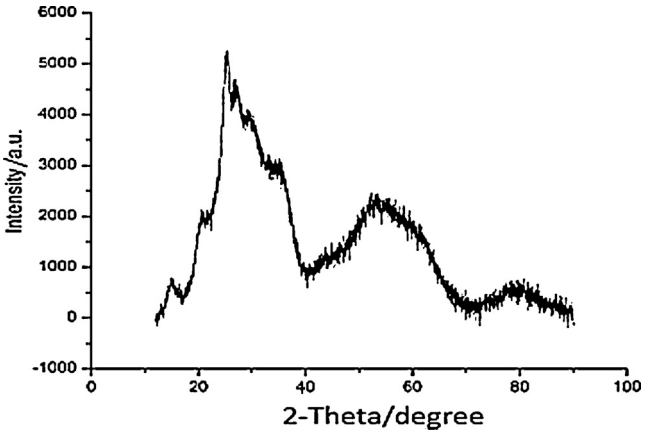

Fig. 8. XRD of tantalum (IV) oxide-**PANi-PSSA**.

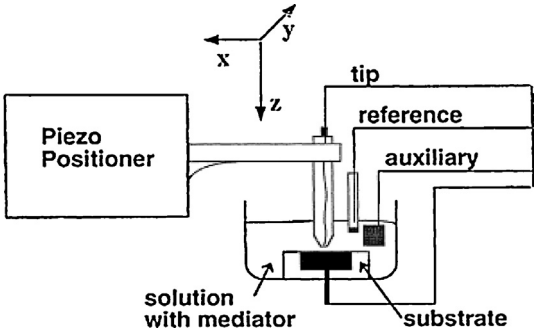

Fig. 9. Block diagram of SECM electrode system [43].

PANi and observed at the wavenumber 1116 cm^{-1} (tantalum (IV) oxide-PANi-PSSA) signify dominance of quinodic ring structure and is a measure of degree of electron delocalization. Any polymer attack occur preferentially on the quinine imine units due to the higher charge localization on the C = N and C = C bonds present in the monomeric units [25–31]. The FTIR data compliments the EDX results and show successful polymerization and doping of PANi by the PSSA. Differences in the FTIR spectra with that of PANi can be explained on the basis of constrained growth and restricted modes of vibration in PANi grown in the presence of metal oxides. In such a case, the aniline monomer gets adsorbed on the oxide particles, which were dispersed in the reaction mixture before initiation of polymerization by ultrasonication and the polymerization proceeds initially on the surfaces of these oxide particles when $(NH_4)_2S_2O_8$ (ammonium persulphate) is added to the solution. This leads to adhesion of the polymer to the metal oxide nanoparticles explaining the constrained growth around the particles. As a result, the characteristic stretching frequencies are shifted towards lower frequency side compared to those of pure PANi. A weak van der Waal's force exist between the polymer chain and the oxide nanoparticles [22]. Also, ionic metal oxide nanoparticles and probably some metallic cations which may form during sonication after some dissolution of some metal oxide nanoparticles might bind to more than one nitrogen site in a PANi chain or form inter-chain linkage among several adjacent PANi chains by coordination. Both intra and inter-chain connections might lead to a more coil-like conformational change or a more twisted aggregation of PANi chains [32].

3.5. UV-visible spectroscopy

The electronic absorption spectrum of the composite is given in Fig. 7.

The spectrum showed three absorption bands showing that the prepared composites not only can strongly absorb the UV light but also can absorb the visible light. These absorption bands are typical of PANi. Peak appearing at about 320 nm can be assigned to π-π* transition of the benzenoid ring while those at about 430 nm and 800 nm can be assigned to polaron-π* and π-polaron band transitions, respectively. These latter two bands are transitions from a localized benzenoid highest occupied molecular orbital to quinoid excitonic transition. This suggests that the composites are PANi composites in its doped state, the emeraldine state [29,33,34]. The rationale behind the use of the UV-Vis spectroscopic technique as a spectroscopical signature [35] for polymers doped with long chain organic acids are structurally modulated and their electronic spectra display additional absorption bands associated with the existence of polarons/bipolarons. The latter bands are delocalization charge defects in the polymer whose presence converts the polymer into an intrinsic conductor. The electronic spectra of undoped polyanilines (prestine) are basically made up of two absorption bands. A band at 320 nm is due to the π-π* transition of the benzoid rings and another at 600 nm assigned to the π-π* of the quinonoid structures [36]. In addition to these bands, organic acid doped polyanilines are characterized by additional bands at 420 and 800 nm associated with the polaron/bipolaron states in the polymer. The latter states are new electronic energy levels created within the polymer sub-gap energies during the polymer/dopants interactions.

3.6. XRD analysis

Fig. 8 shows the XRD diffraction pattern for sulphonated and metal oxide doped PANi composite. The spectrum pattern of the composite exhibit broad peaks at 2-Theta values around 26°, 55°, 80° and a sharp peak appearing at 16° whose degree of sharpness indicates the polycrystalline nature of the composite (Fig. 9).

The peak centred at 16° may be ascribed to the periodicity parallel to the polymer chain while the other peaks may be caused by the periodicity perpendicular to the polymer chain [28,29]. Characteristic peaks of crystalline PANi appear at about 2-Theta = 20°, 26° and 92° [37,38].

Broadening and shifting of peaks occur when Pani forms sulphonated composites with metal oxides. These changes and shifting of peaks suggest that the crystallization of the polyaniline molecular chain is hampered by sulphonation and addition of nanocrystalline metal oxide nanoparticles. This happens when the deposited polyaniline is absorbed on the surface of the oxide

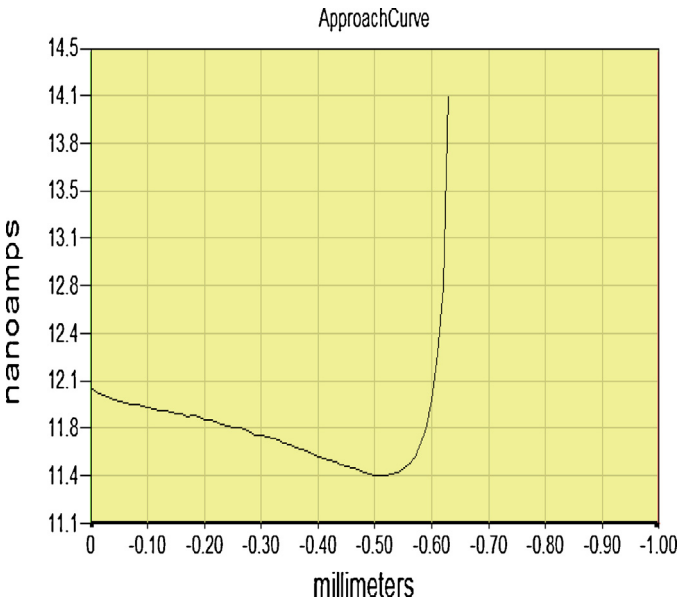

Fig. 10. Approach curve for tantalum (IV) oxide-PANi-PSSA.

nanoparticles. The molecular chain of absorbed polyaniline is tethered and the degree of crystallinity is decreased [33].

3.7. Scanning electrochemical microscopy (SECM) for electrical conductivity analysis

A fast and precise closed loop x, y, z positioning SECM70 workstation electrochemical system with nanometer resolution, along with a flexible data acquisition system [39–42] was used in this work. Its bipotentiostat was used to apply a potential to an Ultra-Micro Electrode (UME) immersed in a solution containing a redox active mediator, potassium ferrocyanide ($K_3Fe(CN)_4$), which is an electroactive species.

The electrode tip generates, via electrolysis, a reduced or oxidized mediator species. When the electrode tip is far from the substrate surface immersed in the solution, the reaction of the redox active dissolved species at the tip results in a faradaic current driven by the hemispherical flux of the substrate from the solution to the tip. A current response was generated at the electrode tip as the tip is moved closer and closer to the substrate in a solution of $Fe(CN)_6^{4-}$. The faradaic current generated was used to study the surface electrical conductivity of the nanocomposite material using the approach feedback mode of the SECM. Fig. 10 is the z-approach curve for tantalum (IV) oxide-PANi-PSSA polymeric nanocomposite. The positive feedback curve profile obtained showed that the material is electrically conductive as explained below.

If sufficiently positive potential is applied to the UME tip, oxidation of Fe^{2+} occurs via the reaction;

$$Fe^{2+}(aq) \rightarrow Fe^{3+}(aq) + e^- \quad (i)$$

The oxidation occurs at a rate governed by diffusion of Fe^{2+} to the UME surface. If the tip is far (i.e. greater than several tip diameters) from the substrate immersed in the electrolyte, a steady state current, i.e. a current at infinite distance from the substrate, flows. This steady-state current ($i_{T,\infty}$) is given by;

$$i_{T,\infty} = 4nFDca \quad (1)$$

Where F is the Faraday constant, n is the number of electrons transferred in reaction (i), D and c are the diffusion coefficient and the bulk concentration of Fe^{2+} respectively and a is the tip radius. When the tip is brought to within a few tip radii of a conductive

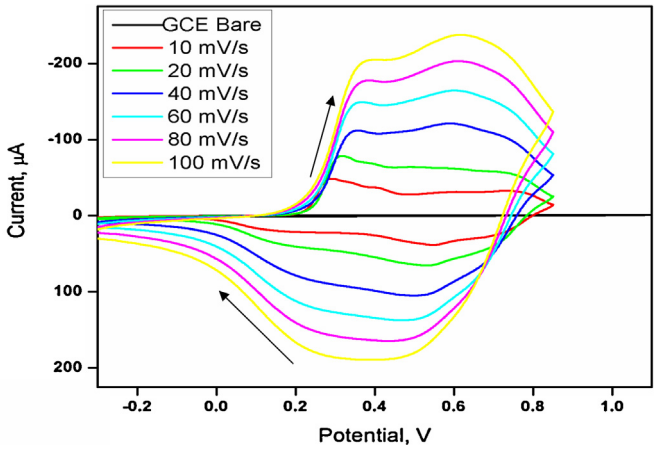

Fig. 11. Scan rate dependence of the cyclic voltammetry of tantalum (IV) oxide-PANi-PSSA.

substrate surface, the Fe^{3+} species diffuses to the substrate where it is reduced back to Fe^{2+} via the reaction;

$$Fe^{3+}(aq) + e^- \rightarrow Fe^{2+}(aq) \quad (ii)$$

The process of equation (ii) produces an additional flux of reduced species to the UME tip making the tip current, i_T, to increase relative to $i_{T,\infty}$, meaning $i_T \square i_{T,\infty}$. The shorter the separation distance (d) between the tip and the substrate, the larger the tip current. As $i_T \rightarrow \infty$, $d \rightarrow 0$. This explains the upward trend of the curve and hence the positive feedback (increasing current as the distance of minimum approach decreases) approach curve profile obtained for the nanocomposite material showing that it is electrically conducting. The rate of the mediator regeneration at the substrate determines the magnitude of the tip current and conversely the dependence of tip-substrate separation.

3.8. Cyclic voltammetry characterization

The oxidative polymerization of aniline and aniline related monomers is a chain reaction whose chain termination step involves the coupling of radical cations to form dimers, oligomers and finally the polymer [44,45]. Fig. 11 is the plot of the cyclic voltammetric responses of the chemically synthesized tantalum (IV) oxide-PANi-PSSA nanocomposite obtained in 1 M H_2SO_4 as the supporting electrolyte at different scan rates. Electroactive species can be oxidized (ox) or reduced (red) and therefore have the ability to pass on an electron(s) from one species to another thus contributing greatly to pseudocapacitance [46]. The multiscan CV curves results of the composite exhibit a complex multi-redox potential electrochemistry having an ability to undergo more than one oxidation or reduction.

Indeed, it has been shown that polyaniline-based systems can exist in three oxidation states, the most reduced polyleucoemeraldine form, the protonated polyemeraldine form (polyemeraldine salt) and the fully oxidized polypernigraniline form [35,47]. Fig. 12 is a cyclic voltammetric cycle of tantalum (IV) oxide-PANi-PSSA at 10 mV/s. It exhibits three characteristic redox couples. At low scan rates, the composite displayed well defined oxidation-reduction responses typical of PANi related composites. The redox couple A/A' could be assigned to the polyleucoemeraldine/polyemeraldine salt transition. The couple at peaks C/C' is the polyemeraldine/polypenigraniline transition [47,48]. The middle redox couple (B/B') has been attributed to the oxidation/reduction of dimers and oligomers entrapped within the polymer matrix or to the degradation products of over-oxidized polyaniline.

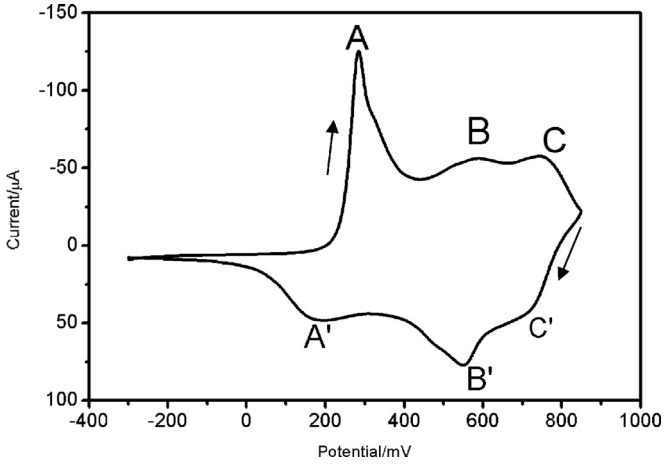

Fig. 12. CV of tantalum (IV) oxide-PANi-PSSA at 10 mV/s.

It has also been attributed to defects in the linear structure of the polymer, or correlated to the formation of cross-linked polyaniline chains by direct reaction of aniline nitrenium cation ($C_6H_5NH^+$) or a reaction between the polyaniline chain itself through the substitution of a nitrenium cation in another polyaniline chain [48–53]. From Fig. 12, the middle peak at B merged with the peak at C at higher scan rates during the oxidative cycles as the peak at A shifted inconsistently towards higher potentials. Also during reductive cycles, the merging together of the peaks at C′ and A′ with the middle peak at B′ with increase in scan rates to form a broad anodic peak centred at the middle of the cyclic voltammetry potential range was accompanied by a shift of the resulting peak towards lower potential values. The shifting of peaks suggests that an irreversible behaviour could be taking place during both oxidative and reductive processes while the merging suggests some sluggish electron transfer processes.

3.9. Design and characterization of supercapacitor cell

In the construction of an electrode, an electrode material with a stable structure must be fabricated and is essential to providing repeatable results. An ideal single electrode should be mechanically strong and electrically conductive. Therefore, the nanocomposite material should be bound into stable matrix with minimum non-conductive polymer binder. A hydrophilic surface is desirable so that aqueous electrolyte can easily penetrate into the pores of the electrode material. A tight contact between the electrode material and the current collector is necessary. Overall, the electrode has to be structurally stable to ensure the repeatability of electrochemical measurements.

3.9.1. Components of electrode materials

The main active electrode material is the chemically synthesized sulphonated-PANi which is doped with the transition metal oxide, tantalum (IV) oxide. This was the polymeric nanocomopsite that was the focus of this investigation. As a conductive material, activated graphitic carbon was added to increase the conductivity of the electrode material [54–57]. As stated earlier, the storage of electric charges in activated carbon is mainly non-faradaic, and the accumulation of ionic charges occurs on a double layer at the electrode/electrolyte interface. The large specific surface area and the porosity of activated carbons are the basic requirements to achieve the quick formation of a double layer; the capacitive behaviours of activated carbons are influenced by their exposed surface area and pore size distribution. In addition, functionalising activated carbon introduced functional groups containing heteroatoms (such as oxygen, nitrogen, sulphur, and halogen). The presence of these functionalities gives activated carbons an acid-base character, which enhances their pseudocapacitive effect. Therefore, tailoring porous structure and surface chemistry of activated carbon is very important to improve electrochemical performance of supercapacitors. Also, these various kinds of functional groups, the acidic surface oxides, serve as adsorption sites for polar molecules [58]. This increases surface hydrophilicity and hence wettability. Surface wettability of the electrode material is important for ensuring the entire pores contact electrolyte for charge storage and or redox activity in the event of pseudocapacitance. Due to the non-conductive nature of PTFE binder, the amount of PTFE added should be limited such that it can bind the particles to stabilize the matrix but still leave the electrode material as conductive as possible. The higher the PTFE content, the higher the resistance of the electrode material. The need to minimize the amount of PTFE is therefore clear. 10% wt of the PTFE was found to bind the material appropriately. From literature, any amount between 4% (the lowest amount reported) and 10% wt is said to be appropriate [57,59,60]. The material of the current collector should be non-corroding in the chosen electrolyte and within the test range of cyclic voltammetry. Nickel mesh is essentially a metal material that cannot store charge, but can be quite resistant to the KOH electrolyte and offers good contact between the active electrode material and the current collector. Otherwise contact resistance greatly affects the performance of an electrochemical capacitor [61,62]. A hydraulic pressure machine was used to apply a pressure of 20 Mpa for 5 min to press the active material onto the nickel mesh. Applying pressure improves the contact between electrode material and current collector and consequently decreases the contact resistance. Moreover, the contact resistance takes up a large percentage of the total internal resistance of the cell. The two-electrode cell system was used to evaluate the performance of capacitor cell, using the BST8-3 eight-channel battery tester. The tester, working at the constant current charge/discharge mode, was used to evaluate the parameters; cell specific capacitance, specific energy, coulombic efficiency and other parameters like the cell stability.

3.9.2. Capacitance measurement with constant current charge/discharge (C/D)

During the test, 0.01 A was used as the average charge/discharge current. The charging and discharging was done within a potential range of 0.0 V to 0.9 V. The choice of the potential range is dictated by the choice of the electrolyte. The choice for the electrolyte was aqueous potassium hydroxide (KOH). Its decomposition voltage limit is theoretically 1.23 V or practically, in kinetic terms, between 1.3 V and 1.4 V. KOH is very soluble in water and because of OH^- anion, have very good conductivities and advantageously high equivalent conductivities in aqueous medium owing to the special mechanism of proton transport (proton hopping) that determines their conductance [63]. Fig. 13 represent the charge/discharge curves from the asymmetric supercapacitor cell configuration assembled using the composite as cathode material and activated carbon as anode material for the first five cycles. Each branch of each circle starts with a voltage drop signifying the *IR* drop, due to the internal resistance of the cell. The different behaviour of the first cycle is always due to the initial starting point where the whole system needs time to reach steady-state behaviour. The discharge segment of the curve was used to calculate the electrical parameters. These were calculated using the following equations [64]; (Figs. 14 and 15)

In the equations, C_s is the specific capacitance in F g^{-1}, E is the specific energy in J g^{-1} and P the specific power in W g^{-1}. The expressions show the discharge current (I) in amperes, the slope of the discharge curve (dV/dt) and mass of the anode (m_a) and cathode (m_c) active materials in grams. The calculation of coulombic

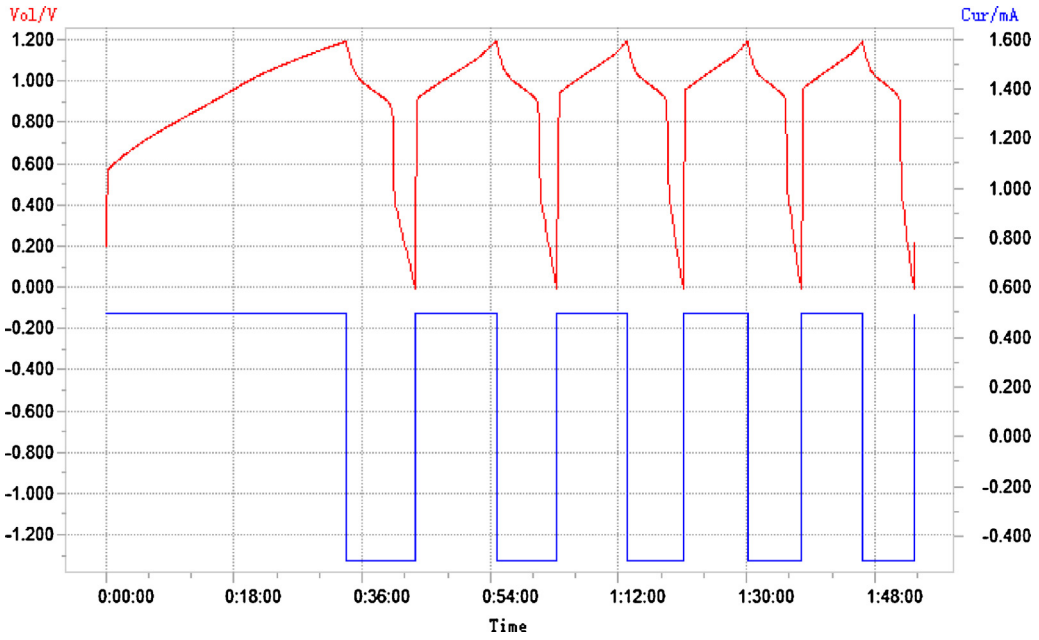

Fig. 13. Charge/discharge curves of TaO_2-PANi-PSSA (1st five cycles).

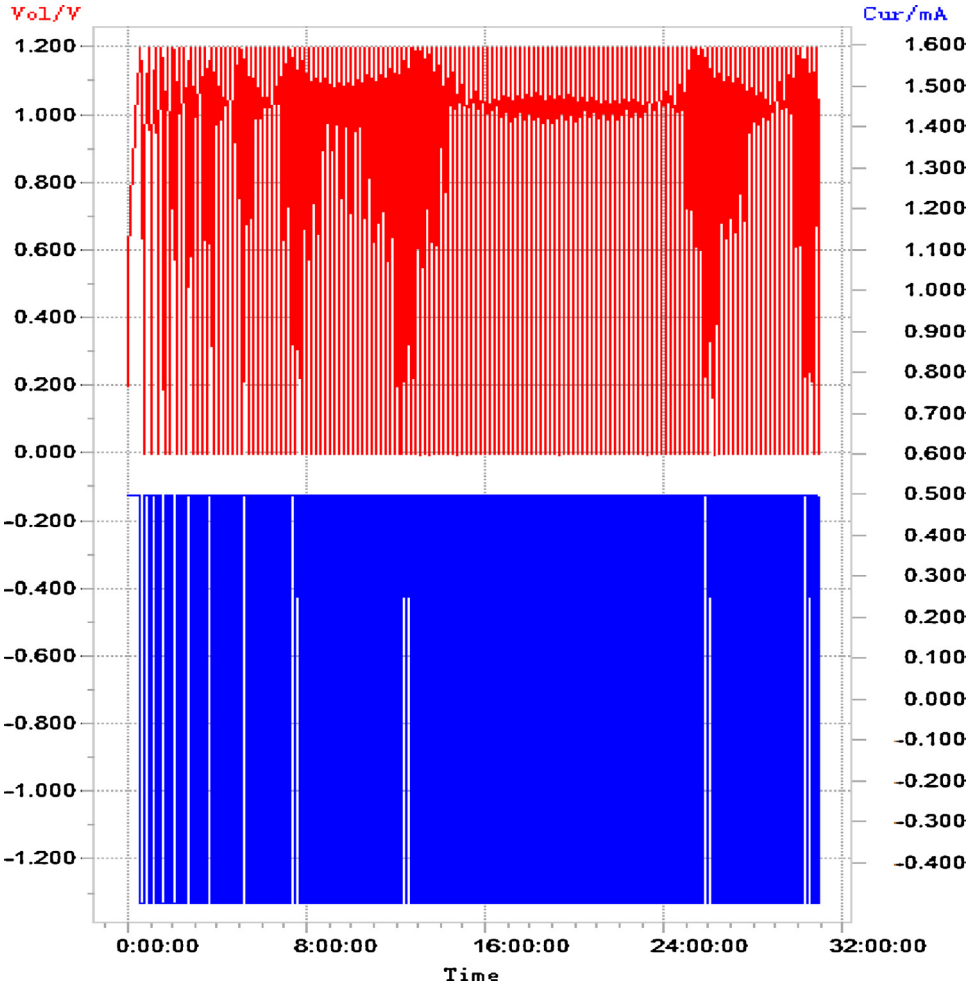

Fig. 14. Voltage-time profile for 143 cycles for tantalum (IV) oxide-PANi-PSSA.

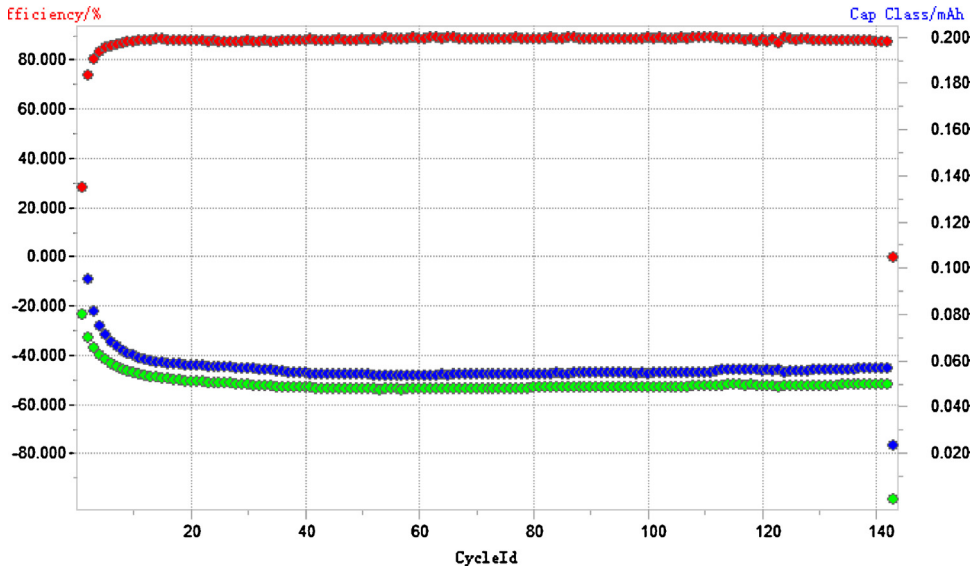

Fig. 15. Coulombic efficiency as a function of the number of cycles for tantalum (IV) oxide -PANi-PSSA.

efficiency was based on the equation, $\eta = \frac{t_D}{t_C} \times 100$where t_C and t_D represent the charging and discharging times, respectively. The values of I, t, V, m_a and m_c were 0.01 A, 296 s, 0.9 V, 0.0216 g and 0.0198 g, respectively. The electrical parameter values computed using the 3rd discharge cycle are: specific capacitance of 318.4 F/g, energy density of 1.57 kWh/kg and power density of 0.435 kW/kg. The cell also demonstrated a high coulombic efficiency value of 94.9%. It can be seen that the charge–discharge profiles deviate from the typical linear variation of voltage with time normally exhibited by electrochemical double layer capacitors (EDLC). The observed non-linearity could be due to the pseudocapacitance arising out of the redox reactions within the potential range used. The values of specific capacitance obtained are within the two electrode capacitance values reported in literature, though comparatively, lower and higher specific capacitance values have been reported at times for single electrode materials [5,8,64–74]. The values obtained depend on several factors key among them is the method used to determine the specific capacitances. When cyclic voltammetric charge is used specific capacitance values depends on the scan rates and increases with increase in scan rates. When a charge-discharge technique is used like the galvanostatic-potentiostatic, the values reported depend on current densities. The values reported in literature are therefore unique to the methods used, conditions of measurements and whether a three or two electrode system was used. The materials are found to be relatively stable over large number of cycles. From the voltage-time profile for tantalum (IV) oxide-PANi-PSSA shown in Fig. 18, the potential remains stable over a large number of cylces meaning that the material does not degrade when cycled many times. They have longer cycle life and therefore a high structural integrity under repeated charging and discharging which is a desirable characteristic of supercapacitor materials. The coulombic efficiency is quite high and remains high as the materials are cycled over and over again as is illustrated in the coulombic efficiency-number of cycles curve profile relating coulombic efficiency, charging and discharging at increasing number of cycles (illustrated in Fig. 19). The efficiency obtained is as high as 94.85%. In the figure, the top curve represent efficiency while the bottom two represents charge during the charging (blue) and discharging (green) regimes. The difference between the bottom two represents charge lost through leakage and hence the inability of the supercapacitor device to contain leakage through self-discharge.

4. Conclusion

Modified sol-gel method produced nanocomposite morphologies of high specific capacitance. Electrode materials and electrolyte need to be optimized and design protocols re-engineered towards reducing internal resistance and hence loss of energy and power since it is an essential ingredient to the performance of the supacapacitor. The nanostructured mixed metal oxides and PSSA doped polyaniline can greatly generate new synergetic properties and improve the overall application performance in supercapacitors that is not available from single metal oxide species and pure PANi due to the appropriate combination of individual ingredients.

Acknowledgement

The authors would wish to acknowledge the National Research Foundation (NRF) of South Africa for financial support.

References

[1] V. Ganesh, S. Pitchumani, New symmetric and asymmetric supercapacitors based on high surface area porous nickel and activated carbon, Journal of Power Sources 158 (2006) 1523–1532.
[2] P.-C. Chen, G. Shen, S. Sukcharoenchoke, C. Zhou, Flexible and transparent supercapacitor based on In_2O_3 nanowire/carbon nanotube heterogeneous films, Applied Physics Letters 94 (2009) 043113–043115.
[3] E. Frackowiak, F. Béguin, Carbon materials for the electrochemical storage of energy in capacitors, Carbon 39 (2001) 937–950.
[4] P. Chen, H. Chen, J. Qiu, C. Zhou, Inkjet printing of single-walled carbon nanotube/ruo_2 nanowire supercapacitors on cloth fabrics and flexible substrates, Nano Research 3 (2010) 594–603.
[5] L.L. Zhang, X.S. Zhao, Carbon-based materials as supercapacitor electrodes, Chemical Society Reviews 38 (2009) 2520–2531.
[6] B.E. Conway, Electrochemical supercapacitors: Scientific Fundamentals and Technological Applications., Kluwer Academic/Plenum Publishers, New York, 1999.
[7] B.E. Conway, V. Birss, J. Wojtowicz, The role and utilization of pseudocapacitance for energy storage by supercapacitors, Journal of Power Sources 66 (1997) 1–14.
[8] A.K. Shukla, S. Sampath, K. Vijayamohanan, Electrochemical supercapacitors: Energy storage beyond batteries, Current Science 79 (2000) 1656–1661.
[9] P. Simon, Y. Gogotsi, Materials for electrochemical capacitors, Nature Materials 7 (2008) 845–852.
[10] E. Frackowiak, Supercapacitors based on carbon materials and ionic liquids, Journal of the Brazilian Chemical Society 17 (2006) 1074–1082.
[11] E. Frackowiak, Carbon materials for supercapacitor application, Physical Chemistry Chemical Physics 9 (2007) 1774–1785.
[12] G. Yu, L. Hu, N. Liu, H. Wang, M. Vosgueritchian, Y. Yang, Y. Cui, Z. Bao, Enhancing the supercapacitor performance of graphene/MnO2 nanostructured electrodes by conductive wrapping, Nano Letters 11 (2011) 4438–4442.

[13] A. Rudge, J. Davey, I. Raistrick, S. Gottesfeld, Conducting polymers as active materials in electrochemical capacitors, Journal of Power Sources 47 (1994) 89–107.
[14] C. Arbizzani, C. Mastragostino, M. Meneghello, Polymer-based redox supercapacitors: A comparative study, Electrochemica Acta 41 (1996) 21–26.
[15] S.K. Dhawan, D. Kumar, M.K. Ram, S. Chandra, D.C. Trivedi, Application of conducting polyaniline as sensor material for ammonia, Sensors and Actuators B: Chemical 40 (1997) 99–103.
[16] A.T. Chidembo, K.I. Ozoemena, B.O. Agboola, V. Gupta, G.G. Wildgoose, R.G. Compton, Nickel(ii) tetra-aminophthalocyanine modified MWCNTs as potential nanocomposite materials for the development of supercapacitors, Energy & Environmental Science 3 (2010) 228–236.
[17] Y.-T. Kim, K. Tadai, A. Mitani, U.-S. Kim, H.-S. Kim, B.-W. Cho, Drastic change of electric double layer capacitance by surface functionalization of carbon nanotubes, Applied Physcs Letters 87 (2005) 234106–234108.
[18] S.-W. Woo, K. Dokko, H. Nakano, K. Kanamura, Incorporation of polyaniline into macropores of three-dimensionally ordered macroporous carbon electrode for electrochemical capacitors, Journal of Power Sources 190 (2009) 596–600.
[19] M. Niederberger, N. Pinna, Metal oxide nanoparticles in organic solvents synthesis: formation, assembly and application. Engineering Materials and Processes Series, 2009, Springer Verlag, London.
[20] J. Stejskal, polyaniline: thin films and colloidal dispersions (IUPAC technical report), Pure and Applied Chemistry 77 (2005) 815–826.
[21] J. Stejskal, M. Spirkova, A. Riede, M. Helmstedt, P. Mokreva, J. Prokes, Polyaniline dispersions 8. The control of particle morphology, Polymer 40 (1999) 2487–2492.
[22] S. Patil, S. Raghavendra, M. Revansiddappa, P. Narsimha, M. Ambika Prasad, Synthesis, transport and dielectric properties of polyaniline/Co_3O_4 composites, Bulletin of Materials Science 30 (2007) 89–92.
[23] K. Gupta, G. Chakraborty, S. Ghatak, P.C. Jana, A.K. Meikap, R. Babu, Synthesis, magnetic, optical, and electrical transport properties of the nanocomposites of polyaniline with some rare earth chlorides, Journal of Applied Physics 108 (2010) 073701–73710.
[24] A. Dey, S. De, A. De, S.K. De, Characterization and dielectric properties of polyaniline-TiO_2 nanocomposites, Nanotechnology 15 (2004) 1277–1283.
[25] A.Y. Arasi, J. Juliet, L. Jeyakumari, B. Sundaresan, V. Dhanalakshmi, R. Anbarasan, The structural properties of Poly(aniline)—Analysis via FTIR spectroscopy, Spectrochimica Acta Part A: Molecular and Biomolecular Spectroscopy 74 (2009) 1229–1234.
[26] A.H. Gemeay, R.G. El-Sharkawy, I.A. Mansour, A.B. Zaki, Preparation and characterization of polyaniline/manganese dioxide composites and their catalytic activity, Journal of Colloid and Interface Science 308 (2007) 385–394.
[27] Y. Fu, Z. Zhao, J. Liu, K. Li, Q. Xu, S. Zhang, Sulfonated polyaniline/vanadate composite as anode material and its electrochemical property in microbial fuel cells on ocean floor, Science China Chemistry 54 (2011) 844–849.
[28] Z. Zhang, Z. Wei, M. Wan, Nanostructures of Polyaniline Doped with Inorganic Acids, Macromolecules 35 (2002) 5937–5942.
[29] D. Wang, F. Ma, S. Qi, B. Song, Synthesis and electromagnetic characterization of polyaniline nanorods using Schiff base through 'seeding' polymerization, Synthetic Metals 160 (2010) 2077–2084.
[30] T. Abdiryim, Z. Xiao-Gang, R. Jamal, Comparative studies of solid-state synthesized polyaniline doped with inorganic acids, Materials Chemistry and Physics 90 (2005) 367–372.
[31] F. Cataldo, P. Maltese, Synthesis of alkyl and N-alkyl-substituted polyanilines: A study on their spectral properties and thermal stability, European Polymer Journal 38 (2002) 1791–1803.
[32] Y. Tan, Y. Zhang, J. Kan, Synthesis and properties on polyaniline in the presence of nickel chloride, eXPRESS Polymer Letters 3 (2009) 333–339.
[33] H. Xia, Q. Wang, Ultrasonic Irradiation: A Novel Approach To Prepare Conductive Polyaniline/Nanocrystalline Titanium Oxide Composites, Chemistry of Materials 14 (2002) 2158–2165.
[34] F.L. Lu, F. Wudl, M. Nowak, A.J. Heeger, Phenyl-Capped Octaaniline (COA): An Excellent Model for Polyaniline, Journal of American Chemical Society 108 (1986) 8311.
[35] A.G. MacDiarmid, Nobel Lecture Synthetic metals: A novel role for organic polymers, Reviews of Modern Physics 73 (2001) 701–712.
[36] T. Hino, T. Namiki, N. Kuramoto, Synthesis and characterization of novel conducting composites of polyaniline prepared in the presence of sodium dodecyl sulphate and several water soluble polymers, Synthetic Metals 156 (2006) 1327–1332.
[37] M. Wan, J. Li, Synthesis and electrical–magnetic properties of polyaniline composites, Journal of Polymer Science Part A: Polymer Chemistry 36 (1998) 2799–2805.
[38] M. Wan, M. Li, J. Li, Z. Liu, Structure and electrical properties of the oriented polyaniline films, Journal of Applied Polymer Science 53 (1994) 131–139.
[39] D.O. Wipf, A. Bard, Scanning electrochemical Microscopy; VII. Effect of electron-transfer rate at the substrate on the tip feedback current, Journal of Electrochemical Society 138 (1991) 469–474.
[40] X. Lu, Q. Wang, X. Liu, Review Recent applications of scanning electrochemical microscopy to the study of charge transfer kinetics, Analytica Chimica Acta 601 (2007) 10–25.
[41] I.C. Jeon, F.C. Anson, Application of scanning electrochemical microscopy to studies of charge propagation within polyelectrolyte coatings on electrodes, Analytical Chemistry 64 (1992) 2021–2028.
[42] M.V. Mirkin, W. Nogala, J. Velmurugan, Y. Wang, Scanning electrochemical microscopy in the 21st century. Update 1: five years after, Physical Chemistry Chemical Physics 13 (2011) 21196–21212.
[43] M.V. Mirkin, B.R. Horrocks, Electroanalytical measurements using the scanning electrochemical microscope, Analytica Chimica Acta 406 (2000) 119–146.
[44] V. Prévost, A. Petit, F. Pla, Studies on chemical oxidative copolymerization of aniline and o-alkoxysulfonated anilines II. Mechanistic approach and monomer reactivity ratios, European Polymer Journal 35 (1999) 1229–1236.
[45] A. Malinauskas, Chemical deposition of conducting polymers, Polymer 42 (2001) 3957–3972.
[46] P.M.S. Monk, Fundamentals of electroanalytical chemistry, Wiley & Sons, New York, 2001.
[47] T. Lindfors, A. Ivaska, pH sensitivity of polyaniline and its substituted derivatives, Journal of Electroanalytical Chemistry 531 (2002) 43–52.
[48] J. Widera, W. Grochala, K. Jackowska, J. Bukowska, Electrooxidation of O-methoxyaniline as studied by electrochemical and SERS methods, Synthetic Metals 89 (1997) 29–37.
[49] J. Yue, Z.H. Wang, K.R. Cromack, A.J. Epstein, A.G. MacDiarmid, Effect of sulfonic acid group on polyaniline backbone, Journal of the American Chemical Society 113 (1991) 2665–2671.
[50] L.-M. Huang, C.-H. Chen, T.-C. Wen, A. Gopalan, Effect of secondary dopants on electrochemical and spectroelectrochemical properties of polyaniline, Electrochimica Acta 51 (2006) 2756–2764.
[51] R. Sivakumar, R. Saraswathi, Redox properties of poly(N-methylaniline), Synthetic Metals 138 (2003) 381–390.
[52] B. Valter, M.K. Ram, C. Nicolini, Synthesis of Multiwalled Carbon Nanotubes and Poly(o-anisidine) Nanocomposite Material: Fabrication and Characterization of Its Langmuir-Schaefer Films, Langmuir 18 (2002) 1535–1541.
[53] E.M. Geniès, M. Lapkowski, J.F. Penneau, Cyclic voltammetry of polyaniline: interpretation of the middle peak, Journal of Electroanalytical Chemistry and Interfacial Electrochemistry 249 (1988) 97–107.
[54] J. Panchompoo, L. Aldous, R.G. Compton, Size-effects in the chemical modification of carbon black nanoparticles with 4-nitroaniline, New Journal of Chemistry 34 (2010) 2643–2653.
[55] C.-C. Yang, S.-T. Hsu, W.-C. Chien, All solid-state electric double-layer capacitors based on alkaline polyvinyl alcohol polymer electrolytes, Journal of Power Sources 152 (2005) 303–310.
[56] J. Li, X. Wang, Y. Wang, Q. Huang, C. Dai, S. Gamboa, P.J. Sebastian, Structure and electrochemical properties of carbon aerogels synthesized at ambient temperatures as supercapacitors, Journal of Non-Crystalline Solids 354 (2008) 19–24.
[57] Y.Z. Wei, B. Fang, S. Iwasa, M. Kumagai, A novel electrode material for electric double-layer capacitors, Journal of Power Sources 141 (2005) 386–391.
[58] K. Miura, T. Morimoto, Adsorption sites for water on graphite. 3. Effect of oxidation treatment of sample, Langmuir 2 (1986) 824–828.
[59] J.H. Park, O.O. Park, K.H. Shin, C.S. Jin, J.H. Kim, An Electrochemical Capacitor Based on a Ni(OH)[sub2]/Activated Carbon Composite Electrode, Electrochemical and Solid-State Letters 5 (2002) H7–H10.
[60] M. Ramani, B.S. Haran, R.E. White, B.N. Popov, L. Arsov, Studies on activated carbon capacitor materials loaded with different amounts of ruthenium oxide, Journal of Power Sources 93 (2001) 209–214.
[61] M. Hahn, M. Bärtsch, B. Schnyder, R. Kötz, M. Carlen, C. Ohler, D. Evard, A 24V bipolar electrochemical double layer capacitor based on activated glassy carbon, in: Power Sources for the New Millenium, The Electrochemical Society, Pennington, NJ, 2001.
[62] J.P. Zheng, Resistance distribution in electrochemical capacitors with a bipolar structure, Journal of Power Sources 137 (2004) 158–162.
[63] B. Conway, Electrochemical Supercapacitors; Scientific Fundamentals and Technological Applications, Kluwer Academic/Plenum Publishers, New York, 1999.
[64] P.-C. Chen, G. Shen, S. Sukcharoenchoke, C. Zhou, Flexible and transparent supercapacitor based on In_2O_3 nanowire/carbon nanotube heterogeneous films, Applied Physics Letters 94 (2009) 043113.
[65] B. Gao, C.-z. Yuan, L.-h. Su, L. Chen, X.-g. Zhang, Nickel oxide coated on ultrasonically pretreated carbon nanotubes for supercapacitor, Journal of Solid State Electrochemistry 13 (2009) 1251–1257.
[66] C. Yuan, L. Chen, B. Gao, L. Su, X. Zhang, Synthesis and utilization of $RuO_2.xH_2O$ nanodots well dispersed on poly(sodium 4-styrene sulfonate) functionalized multi-walled carbon nanotubes for supercapacitors, Journal of Materials Chemistry 19 (2009) 246–252.
[67] V. Gupta, N. Miura, High performance electrochemical supercapacitor from electrochemically synthesized nanostructured polyaniline, Materials Letters 60 (2006) 1466–1469.
[68] C. Yuan, L. Su, B. Gao, X. Zhang, Enhanced electrochemical stability and charge storage of MnO_2/carbon nanotubes composite modified by polyaniline coating layer in acidic electrolytes, Electrochimica Acta 53 (2008) 7039–7047.
[69] J. Ko, K. Ryu, S. Kim, K. Kim, Supercapacitive properties of composite electrodes consisting of polyaniline, carbon nanotube and RuO_2, Journal of Applied Electrochemistry 39 (2009) 1331–1337.
[70] V. Srinivasan, J.W. Weidner, Studies on the Capacitance of Nickel Oxide Films: Effect of Heating Temperature and Electrolyte Concentration, Journal of The Electrochemical Society 147 (2000) 880–885.

[71] E. Frackowiak, V. Khomenko, K. Jurewicz, K. Lota, F. Béguin, Supercapacitors based on conducting polymers/nanotubes composites, Journal of Power Sources 153 (2006) 413–418.
[72] T.C. Girija, M.V. Sangaranarayanan, Polyaniline-based nickel electrodes for electrochemical supercapacitors—Influence of Triton X-100, Journal of Power Sources 159 (2006) 1519–1526.
[73] F. Lisdat, D. Schäfer, The use of electrochemical impedance spectroscopy for biosensing, Analytical and Bioanalytical Chemistry 391 (2008) 1555–1567.
[74] H.-K. Song, H.-Y. Hwang, K.-H. Lee, L.H. Dao, The effect of pore size distribution on the frequency dispersion of porous electrodes, Electrochimica Acta 45 (2000) 2241–2257.